



Random forest model for removal of methylene blue and lead(II) ion using activated carbon obtained from Tamarisk

Farshad Heydari^a, Mehrorang Ghaedi^{b,*}, Amin Ansari^c, Abdol Mohammad Ghaedi^{d,*}

^aDepartment of Chemistry, Fars Science and Research Branch, Islamic Azad University, Marvdasht, Iran, email: Pooya_2831@Yahoo.Com

^bChemistry Department, Yasouj University, Yasouj 75914-35, Iran, Tel./Fax: +98 7432223048; email: M_Ghaedi@Yahoo.Com

^cDepartment of Chemistry, Marvdasht Branch, Islamic Azad University, Marvdasht, Iran, email: Aminansari138@Yahoo.Com

^dDepartment of Chemistry, Gachsaran Branch, Islamic Azad University, P.O. Box 75818–63876, Gachsaran, Iran, Tel. +98 7432332033; Fax: +98 7432332003; email: Abm_Ghaedi@Yahoo.Com

Received 17 March 2015; Accepted 13 September 2015

ABSTRACT

Activated carbon (AC) prepared from the Tamarisk of Iran was used as a novel, local, and nontoxic adsorbent for the removal of methylene blue (MB) and lead(II) ion from aqueous solutions. This new material was prepared in our laboratory using the routine procedure and its surface properties including surface area, pore volume, and functional groups were characterized with various techniques such as BET, FTIR, and scanning electron microscopic analyses. The influence of initial concentration of MB and Pb²⁺ ion, pH, contact time, and adsorbent mass on the adsorption efficiency was investigated and optimized. The evaluation and estimation of equilibrium data from among traditional isotherm models display that the Langmuir model indicated the best fit to the equilibrium data with a maximum adsorption capacity of 27.5 mg g⁻¹, while the adsorption rate efficiently follows the pseudo-second-order model. Two models, namely multiple linear regression and random forest (RF), were used for modeling and optimization of the whole procedure. Results obtained show that the RF model was a powerful tool for the prediction of MB and Pb²⁺ ion adsorption by AC obtained from Tamarisk. The optimal tuning parameters for the RF model were obtained based on $n_{\text{tree}} = 100$ and $m_{\text{try}} = 2$. In the training data-set for MB and Pb²⁺ ion, the mean squared error values of 0.0003 and 0.0002, and the coefficient of determination (R^2) values of 0.9952 and 0.9963 were obtained using the RF model, respectively.

Keywords: Random forest; Removal; Methylene blue; Lead(II) ion; Tamarisk

1. Introduction

The heavy metals (ions) are of the greatest concern and are hazardous and one among the various kinds of environmental pollution (due to their high toxicity and mobility). Their high stability and reactivity in

water sources lead to their accumulation and upon consumption of foods become hazardous to living beings [1]. The release and entrance of heavy metals from industrial activities to aquatic environment cause serious environmental problems in view of human health. These problems call for an urgent need to reduce their concentration and design and develop highly efficient removal procedures. Lead (and/or its

*Corresponding authors.

compound) in addition to dyes is generally applied in storage battery manufacturing, printing, pigments, fuels, photographic materials, and explosives manufacturing [1]. Lead(II) ion as a neurotoxic agent is of major concern and its presence in drinking water (even in low concentrations) is hazardous and leads to problems such as anemia, hepatitis, and nephritic syndrome [2,3]. Exposure to this element and its compounds causes severe health hazards and damages the kidneys, liver, brain, and nervous system, while its long-term exposure may induce sterility, abortion, and neonatal death in humans [4]. Methylene blue (MB) as a basic dye initially was applied for coloring of products such as silk, leather, plastics, paper, and cotton mordant with tannin, as well as in the production of inks and copying paper. The discharge of dyes into environment is a cause of worry in terms of the toxicity and aesthetics. These properties hinder light penetration, subsequently damage water and ecosystem and finally are toxic to organisms in the food chain [5]. Synthetic origin and complex aromatic molecular structures of dyes make biodegradation and photochemical decomposition difficult, while in some cases the final product is more toxic than the original compounds [6]. There are few reports on the simultaneous removal of dyes and metal ions. On the other hand, most widely used techniques for this purpose are ion exchange, chemical co-precipitation, reverse osmosis, evaporation, membrane filtration, and adsorption [7]. Adsorption especially on well-known adsorbents such as activated carbon (AC) enables one to design a process to remove trace amounts of lead and dye from solutions [8–13]. Commercially available ACs despite their original resource suffer from limitations, including high operational cost [14]. AC has a porous structure that renders it a high surface area (greater adsorption capacity) and effective regeneration. High surface reactivity and ability to adsorb and enrich more species are associated with the presence of various functional groups such as carboxylic, carbonyl, lactonic, phenolic, and aldehydic which are located at the edges of a hexagonal carbon layer plane [15]. Ionization of these functional groups in the solution depends highly on pH and subsequently leads to the generation of charge interface between them [16]. The type and magnitude of surface functional groups depend on variables including preparation method and raw materials [17] such as coal, wood, peat, and coconut shells [18]. However, the demand for new, cheap, efficient, and simply regenerable adsorbents initiated a novel pathway to apply locally available and renewable materials as potential alternative precursors for producing AC. For this purpose, many materials such as fruit stones [19], pyrolyzed coffee

residues [20], pine bark [21], nutshells [22], and olive stones [23] were studied. Engineering is the application of physical and mathematical sciences to solve problems following experimental testing that in engineering is normally an expensive and time-consuming task. These problems can simply be resolved by application of computational models derived from engineering experimental data. Modeling is a simplification of reality that is a well-accepted engineering technique, which is very helpful for the successful analysis of behavior of each process and to confirm its results. The selection of suitable methods for constructing models is a crucial and vital role that improves repeatability and accuracy of the process. Wide-application statistical methods are classified into the following branches: multiple linear regression (MLR) [24] and nonlinear, artificial neural networks [25,26], fuzzy inference system (FIS), adaptive neuro-fuzzy inference system (ANFIS) [27], support vector machine (SVM) [24], and random forest (RF) [28]. Among these, RF as a relatively new nonlinear method is applicable in classification and regression problems. In our previous work, MLR and RF models were used for the removal of bromophenol blue (BPB) using AC achieved from the *Astragalus bisulcatus* tree. The results indicated that the RF model was a powerful tool for the prediction of experimental data concerning BPB adsorption. The optimal tuning parameters for the RF model were obtained based on $n_{\text{tree}} = 100$ and $m_{\text{try}} = 2$. For the training data-set, the mean-squared error (MSE) values of 0.0006, and the coefficient of determination (R^2) values of 0.9895 for the RF model, and the MSE value of 0.0104, and the R^2 value of 0.823 for the MLR model were obtained [28]. Philibert et al. used the RF model to predict the emission of N_2O with local information following N fertilization using the RF model and the type of crop and experiment duration as its input variables [29]. Schwartz et al. applied the RF algorithm to forecast the consequences of intramuscular psoas lengthening as part of a single-event multi-level surgery in patients with cerebral palsy [30]. Adusumilli et al. developed a RF regression integrating low-cost inertial navigation system and global positioning system (INS/GPS). Their results show that RF regression can effectively model the highly nonlinear INS error because of its increased generalization capability. The result of the proposed model illustrates a significant reduction in the positional error by 24–56% [31]. In this study, MLR and RF models have been used for the prediction of the adsorption of MB and Pb^{2+} ion by AC obtained from Tamarisk, which was preliminarily characterized via different techniques including BET, FTIR, and scanning electron microscopic (SEM)

analyses. Then, the kinetics and isotherms of their adsorption onto this novel AC were studied. The adsorption rates were estimated by fitting the experimental data to conventional kinetic models including pseudo-first- and second-order and intraparticle diffusion models.

2. Experimental

2.1. Materials and methods

RF is an ensemble machine-learning technique that is applied to improve the classification and regression trees (CART) using a combination of hundreds of unpruned decision trees [32]. The goal of RF is to decrease the correlation between individual trees using bootstrapping and the randomized variable selection method, and subsequently diminish variance. The RF algorithm requires the following tuning parameters: n_{tree} , the number of regression trees, which increase based on a bootstrap sample of the original data-set (the default value is 500 trees); m_{try} , the number of various predictors to try at each node (the default value is one-third of the total number of variables); and node size, the minimum size of terminal nodes. The larger the number of node size, the smaller the trees (the default values are one and five for classification and regression, respectively). The RF regression model accomplishes as follows (for more details, see reference [32]): the first step of the method is random selection (generally, about two-thirds of the initial sample are selected in a bootstrap sample (called the in-bag samples)). Subsequently, one-third of the initial samples is left out (called the out-of-bag (OOB) samples). In this study, 70 and 30% of initial samples were selected for OOB and in-bag samples, respectively. The second step is based on the appropriate selection of m_{try} . In the RF model following a good selection, the tuning parameter m_{try} has to be small and avoiding overfitting. The third step includes the best selection of n_{tree} to construct a tree (based on variables in-bag and m_{try}). Optimum n_{tree} is a point at which error no longer decreases. The tree-partitioning algorithm is constructed by recursively partitioning the larger spaces into two smaller spaces. The selection of split point is an optimization problem based on the squared error loss that is simply carried out by application of the algorithm to the root node. The most common stopping criterion is to keep the number of samples in a lower value and fall in the R_m region (disjoint subspaces of the input space). In the RF model, overfitting occurs in cases of complex regression trees. For example, if m_{try} is large, it is possible that at each generation, the regression tree

output grows too large. The experimental data-set is randomly divided into training and testing sets (252 and 108 were applied for training and testing, respectively). All computations were performed with the RF-Matlab package created by Abhishek Jaiantilal (<https://github.com/jrderuiter/randomforest-matlab>). The inputs consist of concentration (mg L^{-1}), amount of adsorbent (g), and contact time (min). The output is the removal (%). Inputs and outputs are normalized between 0.1 and 0.9 to avoid numerical overflows due to very large or small weights. The normalization equation used is as follows:

$$y = (x_i - x_{\min}/x_{\max} - x_{\min}) \times 0.8 + 0.1 \quad (1)$$

where y is the normalized value of x_i , while x_{\max} and x_{\min} are the maximum and minimum values of x_i , respectively. The performance and accuracy of the RF model for accurate prediction of the optimum value of all variables and strong modeling adsorption behavior are judged by considering variables such as MSE and coefficient of determination (R^2) that are simply presented via the following equation:

$$\text{MSE} = \frac{1}{N} \sum_{i=1}^N \left(|y_{\text{prd},i} - y_{\text{exp},i}| \right)^2 \quad (2)$$

$$R^2 = 1 - \frac{\sum_{i=1}^N (y_{\text{prd},i} - y_{\text{exp},i})^2}{\sum_{i=1}^N (y_{\text{prd},i} - y_m)^2} \quad (3)$$

where $y_{\text{prd},i}$ is the predicted value of the RF model, $y_{\text{exp},i}$ is the experimental value, N is the number of data, and y_m is the average of the experimental value.

2.2. Multiple linear regressions (MLR)

MLR models are commonly applied in environmental studies in order to model the change and dependency of numerous independent variables to the dependent variable according to the following mathematical equation:

$$Y = b_0 + b_1X_1 + b_2X_2 + \dots + b_nX_n \quad (4)$$

where Y is the predicted value of the MLR model, b_i ($i = 0, \dots, n$) are the regression coefficients, and X_i ($i = 1, \dots, n$) are the independent variables (inputs). The MLR model is easy to use in determining the cumulative influence of variables such as time, adsorbent dosage, and dye concentration of the system on the removal percentage. In the study, SPSS 15 statistical program has been used for the MLR model.

2.3. Instruments and reagents

Stock solutions (200 mg L^{-1}) of MB (Fig. 1) (Chemical formula of $\text{C}_{27}\text{H}_{34}\text{N}_2\text{O}_4\text{S}$; CI = 42,040; FW = $482.64 \text{ g mol}^{-1}$ known as basic green 4 with λ_{max} of 623 nm) were prepared by dissolving 20 mg of pure compound in 100 ml of double-distilled water, while working solution was prepared freshly. A stock solution of Pb^{2+} ions ($1,000 \text{ mg L}^{-1}$) was prepared by dissolving 0.4 g of its nitrate salt (supplied from Merck, Dermasdat, Germany) in distilled water. The stock solution was diluted with distilled water to obtain working solutions with desired concentrations.

The pH of the solutions was adjusted to the required value using a dilute solution of NaOH and/or HNO_3 , while it was measured using pH/Ion meter model-691 (Metrohm, Switzerland, Swiss). The absorbance was recorded by Jusco UV-vis spectrophotometer model V-530 (Jasco, Japan) at 664 nm. The morphology of AC-Tamarisk was followed by field emission scanning electron microscopy (FE-SEM; Hitachi S-4160, Japan) at an acceleration voltage of 15 kV. X-ray diffraction pattern was obtained with an automated Philips X'Pert X-ray diffractometer with Cu-K α radiation (40 kV and 30 mA) for 2θ values over $10\text{--}70^\circ$. A BET surface analyzer (Quantachrome NOVA 2000, USA) was used to determine nitrogen adsorption-desorption isotherm at 77 K. Before each study, the samples were degassed via helium purging at 553 K for 3 h. The BET experiments give useful information on the adsorbent properties including surface area, total pore volume, and micropore area. Fourier transform infrared (FT-IR) analysis for characterization of AC-Tamarisk was performed using a KBr disk (Shimadzu FTIR-8300 spectrophotometer, Shimadzu Co., Tokyo, Japan).

2.4. Measurements of dye and Pb^{2+} ion uptake

The dye and Pb^{2+} ion concentrations were determined according to calibration curves achieved by tracing the absorbance vs. their initial concentration at respective maximum wavelengths. The dependency of MB and Pb^{2+} ions removal percentage was determined over 2–60 min, while equilibrium was established after

30 min for MB and 45 min for Pb^{2+} ions. The effect of initial pH (1–8) on the compounds removal was studied by contacting 50 mL of 15 mg L^{-1} with 0.015 g of AC-Tamarisk following 60 min of contact time. The equilibrium and isotherm studies were investigated at the concentration range of $5\text{--}40 \text{ mg L}^{-1}$, while the mathematical equation used for the required concepts is as follows:

$$\% \text{ MB and } \text{Pb}^{2+} \text{ ion removal} = ((C_0 - C_t)/C_0) \times 100 \quad (5)$$

$$q_e = (C_0 - C_e)V/W \quad (6)$$

where C_0 (mg L^{-1}) and C_t (mg L^{-1}) are the concentrations of target at initial and after time t , respectively. V (L) is the volume of the solution and W (g) is the mass of the adsorbent.

2.5. Preparation of AC by Tamarisk

Two kilograms of the stem wood of the Tamarisk tree was ground into small portions, and washed two times, and was cooked, and heated at 350°C in a 1.0-L vessel for 3 h to eliminate water-soluble phenolic compounds and to elude their releases during adsorption experiments. Subsequently, the product wastes were washed with distilled water and dried at 150°C in an air-supplied oven for 12 h and thereafter, they were sieved in a mesh in the range of 50–80 and subsequently was carbonized under argon atmosphere with a heating rate of 5°C min^{-1} until 500°C and kept at this temperature for 1 h. The mass was then cooled and washed thoroughly several times with distilled water and dried and fully characterized with different conventional techniques, such as SEM and BET analyses. The point of zero charge pH (pH_{ZPC}) was examined via a well-known pH drift method, and some of its predetermined properties are presented in Table 1.

3. Results and discussions

3.1. Characterization of adsorbent

The specific surface area of AC prepared from the Tamarisk tree evaluated by BET was found to be $26.46 \text{ m}^2 \text{ g}^{-1}$, and its pore diameter was lesser than 22.4 nm, and AC poses a total pore volume of lesser than 0.5 mL g^{-1} with abundance around 60% (high mesopore volume) (Table 2 and Fig. 2(a)). The pores between 100 and 200 nm have a total volume around $0.006532 \text{ cm}^3 \text{ g}^{-1}$ with a frequency around 42% (macropores). The FT-IR spectra (Fig. 2(b)) reveal some absorption peaks belonging to OH groups in the

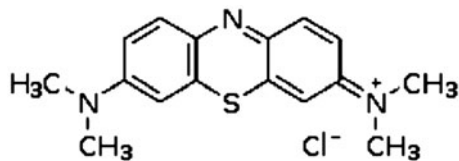


Fig. 1. The structure of MB.

Table 1
Characteristics of the prepared AC of Tamarisk

Property	Values
Elements present (%)	C: 76; O: 22; Al: 0.5; Cl: 1.5
BET specific surface area (m ² g ⁻¹)	27.798
Alkali soluble	1.0 wt%
Water soluble	0.3%
Acid soluble	1.0 wt%
pH _{ZPC}	5.5

range of 3,300–3,400 cm⁻¹, while the bands at about 2,900 cm⁻¹ are assigned to the aliphatic C–H groups and the peak at the position of 1,725 cm⁻¹ could be due to the carbonyl stretch of carboxyl. The trough around 1,600 cm⁻¹ represents the C=O stretching. Symmetric bending of CH₃ was observed to shift around 1,450 cm⁻¹ and the peaks at about 1,050 and 1,200 cm⁻¹ support the presence of C–O stretching and SO₃ stretching of other groups, respectively. The peaks observed at around 1,500 cm⁻¹ correspond to the secondary amine group.

The SEM is the primary tool used for the characterization of the surface morphology and fundamental physical properties of photocatalyst surfaces. It is useful for the determination of particle size, shape, and porosity. The SEM photograph was recorded using FE-SEM (Hitachi S-4160, Japan). The FESEM images of the AC surface are shown in Fig. 3. It can be seen that the surface morphology of AC is homogeneous and relatively smooth; the SEM micrograph of the adsorbent (1.57K× magnification) shows and confirms the homogeneous structure and appearance of different pores that allow successful application in the adsorption of different compounds (Fig. 3).

Table 2
Summary report of adsorbent properties

<i>Surface area</i>	
BET surface area	26.4637 m ² g ⁻¹
Langmuir surface area	33.2753 m ² g ⁻¹
BJH adsorption cumulative surface area of pores between 17.000- and 3,000.000-Å width	0.213 m ² g ⁻¹
<i>Pore volume</i>	
BJH adsorption cumulative volume of pores between 17.000- and 3,000.000-Å width	0.006532 cm ³ g ⁻¹
<i>t</i> -Plot micropore volume	0.01643 cm ³ g ⁻¹
<i>Pore size</i>	
Adsorption average pore width (4 V/A by BET)	1,769.713 Å
<i>Nanoparticle size</i>	
Average particle size	2,243.7856 Å

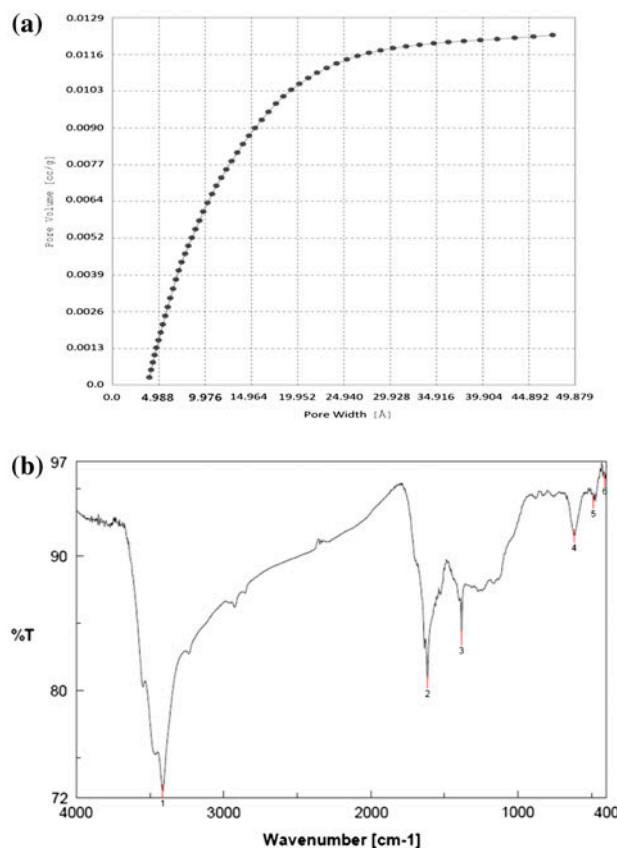


Fig. 2. (a) Pore size distribution and (b) FT-IR study of AC.

3.2. RF model

RF effectively has three tuning parameters, namely n_{tree} , m_{try} , and extra options. The range of tuning parameters, the obtained coefficient of determination (R^2) and MSE for the training set and testing set

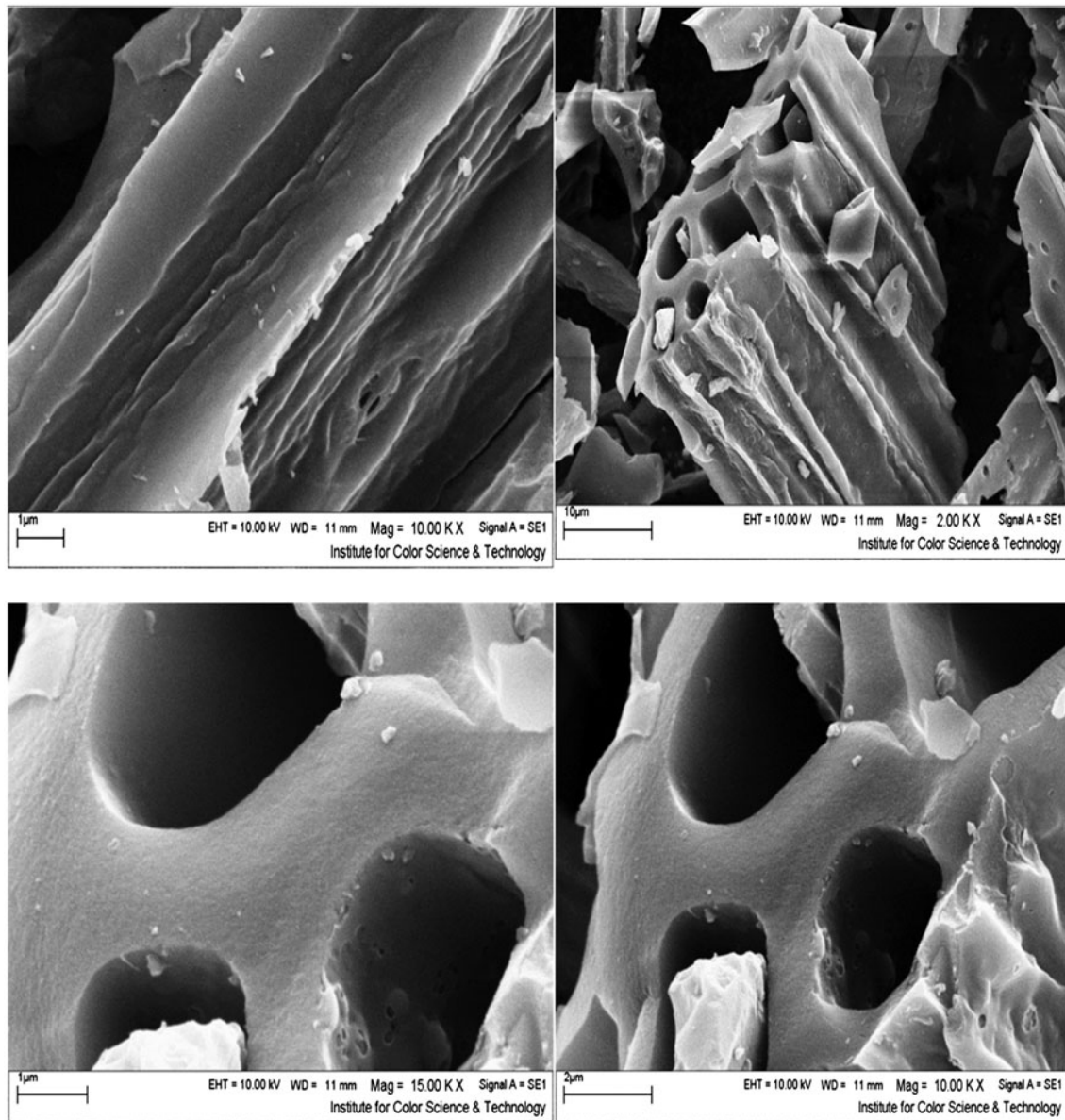


Fig. 3. FESEM images of AC (Tamarisk).

confirm that optimal tuning parameters of the RF model for MB are obtained based on the $n_{\text{tree}} = 100$, $m_{\text{try}} = 2$, importance = 1, and nPerm = 3 (extra options: nPerm = number of times the OOB data are permuted per tree for assessing variables). The above-mentioned parameters for Pb^{2+} ion are achieved based on $n_{\text{tree}} = 100$, $m_{\text{try}} = 2$, and extra options of default (with replacement) in the forest. For MB and Pb^{2+} ion in the optimal RF model, the MSE values were 0.0003, 0.0006, 0.0002, and 0.0004, respectively. On the other hand, the R^2 values were 0.9952 and 0.9872 for MB and 0.9963

and 0.9885 for Pb^{2+} ion for the training and testing sets, respectively (Table 3). Fig. 4(a) and (b) exhibits the performance of the optimal RF model for the data-sets of MB and Pb^{2+} ion, respectively. As can be seen from these figures, there is a good agreement between experimental and predicted data using the RF model for both adsorbates. The out-of-bag (OOB) error rate vs. the number of trees is plotted for both adsorbates (Fig. 5). It can be observed the out-of-bag error rate converges at a point after 200 trees and remains constant and adding more trees does not help.

Table 3

Range of tuning parameters and obtained statistical data for training and testing data-sets of MB and lead(II) ion

	n_{tree}	m_{try}	Extra_options	Methylene blue				Lead(II) ion			
				Training set		Testing set		Training set		Testing set	
				R^2	MSE	R^2	MSE	R^2	MSE	R^2	MSE
1	500	1	–	0.9815	0.0025	0.9735	0.0036	0.9810	0.0026	0.9619	0.0028
2	100	1	–	0.9751	0.0029	0.9675	0.0040	0.9835	0.0027	0.9664	0.0028
3	100	2	–	0.9942	0.0003	0.9844	0.0007	0.9963	0.00019	0.9885	0.00044
4 ^a	500	1	–	0.9812	0.0027	0.9733	0.0038	0.9810	0.0026	0.9619	0.0028
5 ^b	100	4	Without replacement	0.9774	0.0025	0.9619	0.0036	0.9783	0.0026	0.9538	0.0030
6	100	4	Sample size = size(X_trn, 1) × 2/3	0.9761	0.0030	0.9749	0.0035	0.9787	0.0032	0.9582	0.0033
7 ^c	100	4	Node size = 7	0.9715	0.0030	0.9669	0.0041	0.9789	0.0028	0.9644	0.0028
8 ^d	100	4	Importance = 1	0.9808	0.0028	0.9722	0.0041	0.9816	0.0027	0.9635	0.0028
9 ^d	100	4	LocalImp = 1	0.9803	0.0027	0.9705	0.0036	0.9816	0.0027	0.9635	0.0028
10 ^d	100	4	Proximity = 1	0.9756	0.0027	0.9651	0.0039	0.9835	0.0026	0.9664	0.0028
11 ^e	100	4	Proximity = 1 oob_prox = 0	0.9807	0.0025	0.9681	0.0039	0.9835	0.0026	0.9664	0.0028
12 ^d	100	4	Do_trace = 1	0.9780	0.0027	0.9729	0.0036	0.9835	0.0026	0.9664	0.0028
13 ^d	100	4	Inbag = 1	0.9815	0.0023	0.9708	0.0035	0.9835	0.0026	0.9664	0.0028
14 ^d	100	2	Importance = 1 nPerm = 1	0.9778	0.0027	0.9710	0.0037	0.9810	0.0027	0.9664	0.0028
15	100	2	Importance = 1 nPerm = 3	0.9952	0.0003	0.9872	0.0006	0.9961	0.00021	0.9876	0.00048

Note: Values in bold indicate the best model.

^aSet to default trees and m_{try} by specifying the values as 0.^bSet sampling without replacement (default is with replacement).^cNote that the default value is 5 for regression.^dDefault (Don't) = 0.^eDefault = 1, if proximity is enabled, Don't = 0.

3.3. MLR model

MLR approach is used to study the presence of linear relationship between normalized inputs and removal percentage. MLR models for training sets were obtained using three inputs and Eqs. (7) and (8) were obtained for the prediction of MB and Pb²⁺ ion removal percentage, respectively, as follows:

$$Y = 0.523 + 0.357x_1 - 0.460x_2 + 0.319x_3 \quad (7)$$

$$Y = 0.313 + 0.179x_1 - 0.259x_2 + 0.654x_3 \quad (8)$$

where Y , x_1 , x_2 , and x_3 are the removal percentage, adsorbent dosage (g), initial dye concentration (mg L⁻¹), and contact time (min), respectively. Finally, the above models were applied to predict the actual removal percentage of experiments concerning testing sets. Fig. 6(a) and (b) shows the simulated values of normalized removal of data in the training and testing sets using the MLR models and their plotting vs. normalized experimental data for MB and Pb²⁺ ions,

respectively. The statistical results of the MLR models exhibit a coefficient of determination (R^2) of 0.879 and 0.835, and a MSE of 0.0048 and 0.3438 for their training data-set (for MB and Pb²⁺ ions). The MLR model was also evaluated on the testing set; the results show an R^2 of 0.859 and 0.841 and a MSE of 0.0055 and 0.3235 for MB and Pb²⁺ ions, respectively.

3.4. Comparison of presented models

Two different models (MLR and RF) are used for the assessment of data-sets and their performances are compared and summarized in Table 4. The results indicate the better ability of the RF model for more accurate and repeatable prediction of experimental data.

3.5. Effect of pH on Pb²⁺ ions and MB removal percentage

Generally, the pH of a solution is recognized as one of the parameters highly effective on the efficiency of the adsorption process that is attributed to its

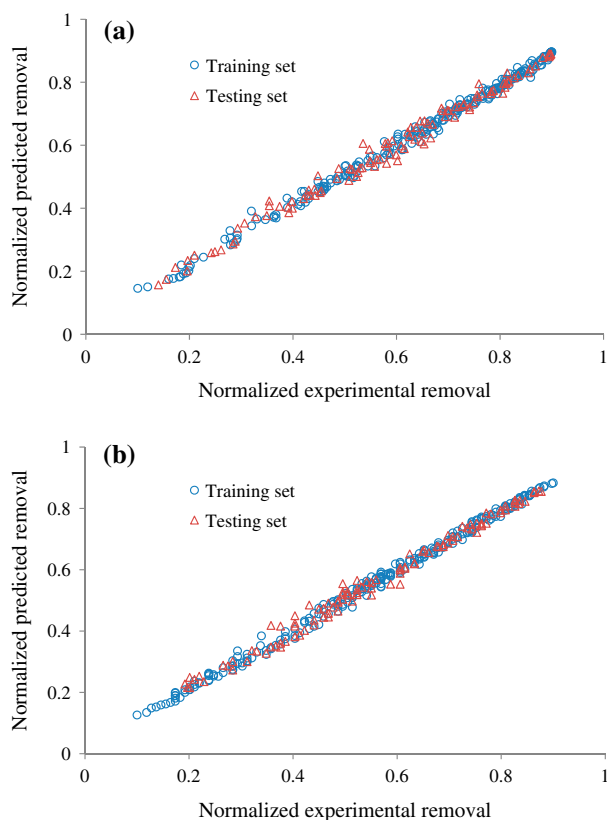


Fig. 4. Experimental data vs. predicted data of normalized removal obtained with RF models, (a) MB and (b) lead(II) ion.

unique role in the surface charge process of the adsorbent and the abundance and nature of analyte species. The chemical reaction (protonation and deprotonation) of functional groups and the competition of metal ions and dyes for binding to the reactive sites of adsorbent can be strongly influenced by pH [33]. The effect of pH on the adsorption of Pb^{2+} ions and MB onto AC-Tamarisk was investigated in the pH range of 1.0–9.0 (15 mg L⁻¹ of MB and Pb^{2+} ions at 0.2 g of AC) at room temperature ($27 \pm 2^\circ\text{C}$), an agitation speed of 300 rpm, and a contact time of 60 min (Fig. 7). The Pb^{2+} ion removal percentage has a positive correlation and an increasing trend with pH up to 5.0 and then remains practically constant. Therefore, pH 5.0 was considered as the optimum pH to obtain maximum adsorption by AC-Tamarisk. At higher pH values, adsorbent gets a neutral charge and a simultaneous contribution of pathways such as electrostatic attraction, π - π interaction, ion-dipole interaction, van der Waals forces, and hydrogen bonding makes it possible to achieve a high target compounds removal percentage [34].

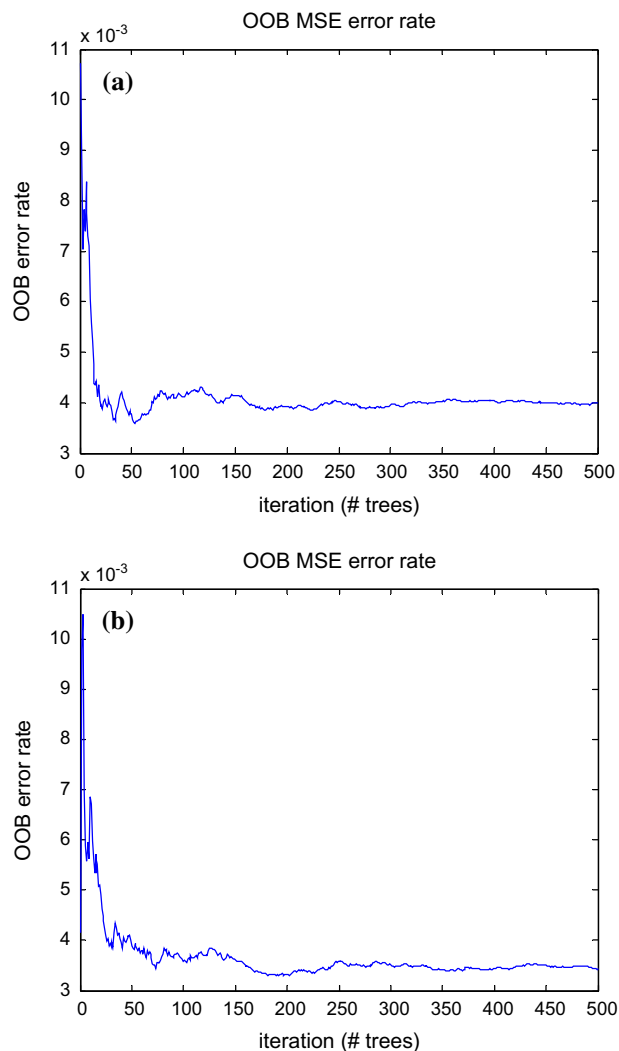


Fig. 5. OOB error rate vs. number of trees, (a) MB and (b) lead(II) ion.

Similar values of optimum pH for the sorption of the Pb^{2+} ion are reported in the literature using cone biomass of *P. sylvestris* [35] and pH 5.0 using maple sawdust [36] and activated sawdust [37]. The decrease in the adsorption capacity of AC-Tamarisk at lower pH can be attributed to the competition of H^+ ions with both cationic species for binding onto the adsorbent surface [36].

3.6. Effect of adsorbent dose

The extent of adsorption of MB and Pb^{2+} ions onto AC-Tamarisk was studied at different adsorbent doses (0.2, 0.3, 0.4, and 0.5 g), various initial concentrations (5–30 mg L⁻¹), pH 5, and room temperature. It is evident (Fig. 8) that MB and Pb^{2+} ions have a similar

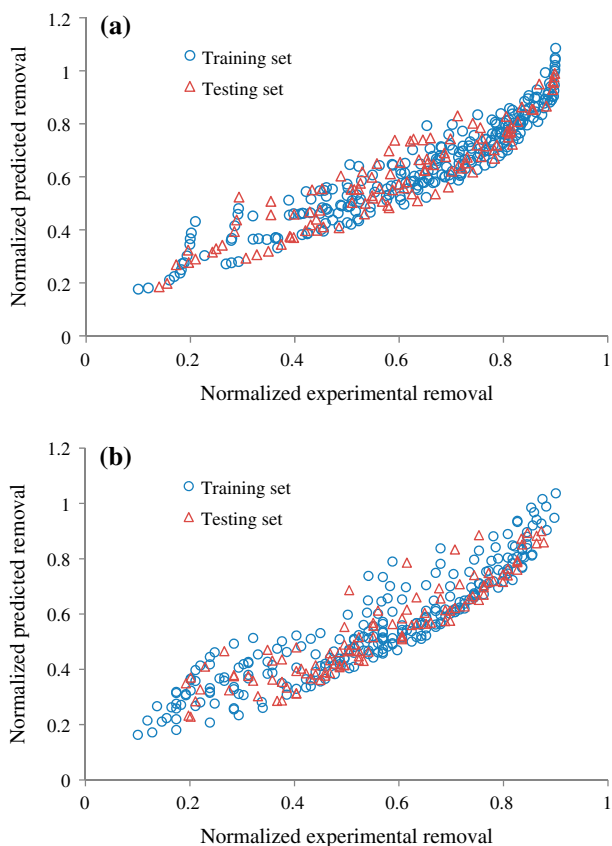


Fig. 6. Experimental data vs. predicted data of normalized removal obtained with MLR models: (a) MB and (b) lead (II) ion.

trend with adsorbent mass. Raising the adsorbent amount (higher number of reactive sites) leads to an enhancement in the interaction of target compounds with the proposed adsorbent through pathways such as soft–soft interaction, π – π , and hydrogen bonding [38,39]. Therefore, increasing the adsorbent amount leads to an increase in the available surface area and adsorption sites (an increase in the amount of mass transfer). A change in the magnitude of AC dosage from 0.1 to 0.5 g causes a significant improvement in removal percentage from 40 to 96% for MB and from

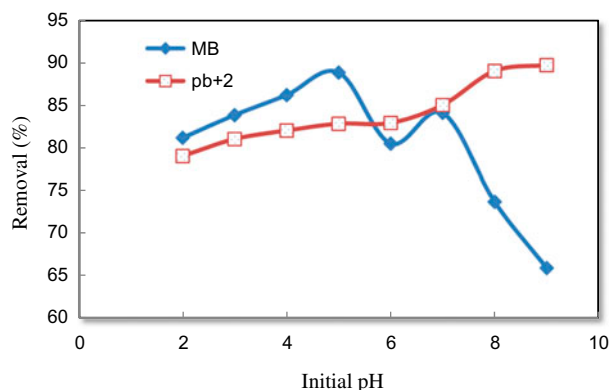


Fig. 7. Effect of pH on the adsorption of MB and Pb²⁺ ions onto AC-Tamarisk.

0.35 to 98% for Pb²⁺ ions, while the adsorption capacity decreased [34].

3.7. Effect of contact time and initial concentration on adsorption of species

Fig. 9 shows the dependency between the removal percentages MB and Pb²⁺ ions and their initial concentration at different contact times, while in all cases the enhancement in the removal percentage with contact time was seen until 60 min. The adsorption process is characterized by a rapid uptake of the adsorbate as shown by the curves. The adsorption rate, however, increased marginally after the first 30 min to a near-constant value with increased contact time. This trend agrees with the report of other investigators [40–42]. The percent adsorbed was maximum at 60 min mostly at initial concentrations; hence, 60 min was the optimum contact time for the adsorption of MB and Pb²⁺ ions onto the prepared carbon. The optimum concentration for the adsorption of MB and Pb²⁺ ions onto the prepared AC was found to be 15 mg L⁻¹ for MB and 20 mg L⁻¹ for Pb²⁺ ions. The optimum concentration of the dye and ion refers to the concentration at which the maximum removal of dye and ion was noticed (Fig. 10) [42]. The percentage removal,

Table 4
Comparison of MSE and R² obtained using the MLR and RF models

Model	Methylene blue				Lead(II) ion			
	Training set		Testing set		Training set		Testing set	
	R ²	MSE	R ²	MSE	R ²	MSE	R ²	MSE
RF	0.9952	0.0003	0.9872	0.0006	0.9963	0.00019	0.9885	0.00044
MLR	0.879	0.0048	0.859	0.0055	0.835	0.3438	0.841	0.3235

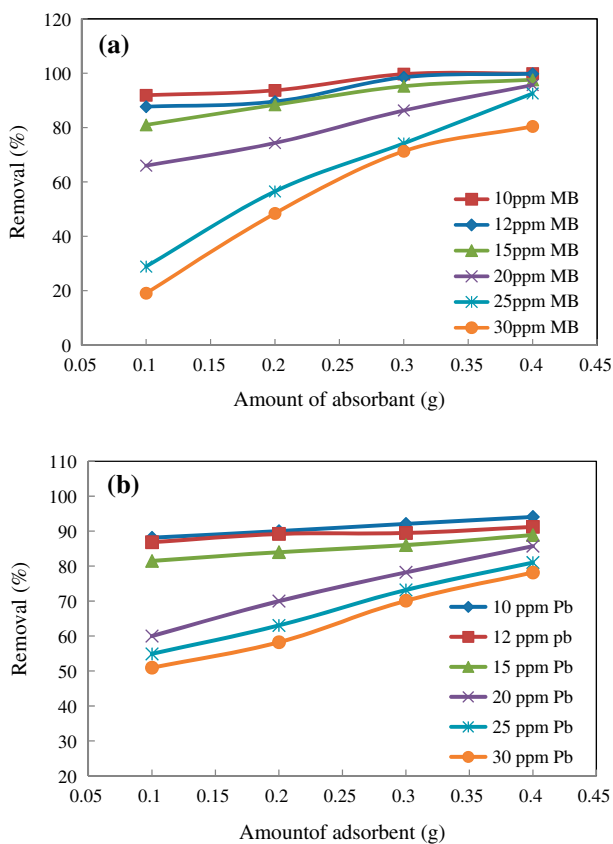


Fig. 8. Effect of adsorbent dosage on the removal of (a) MB and (b) Pb²⁺.

however, decreased with an increase in the initial concentration of MB and Pb²⁺ ions. This may be attributed to a lack of available active sites required for the high initial concentration of the dye and ion [42]. The adsorption sites took up the available solute more quickly at lower concentrations [43]. The percent adsorbed decreased from 91 to 68% after the first 30 min of contact time of MB and from 87 to 56% after the first 30 min of contact time of Pb²⁺ ions with the adsorbent as the initial concentration increased from 5 to 30 mg L⁻¹. At the optimum contact time of 50 min, the percent of adsorbed decreased from 99 to 95 percent, while the amount of adsorbent increased from 0.1 to 0.4 g for MB and Pb²⁺ ions. It is generally observed that the amount of adsorbed increased with an increase in contact time and initial concentrations [41,44].

3.8. Adsorption kinetics

A kinetic study of adsorption is necessary as it provides the information about the adsorption mechanism, which is crucial for the practicality of the pro-

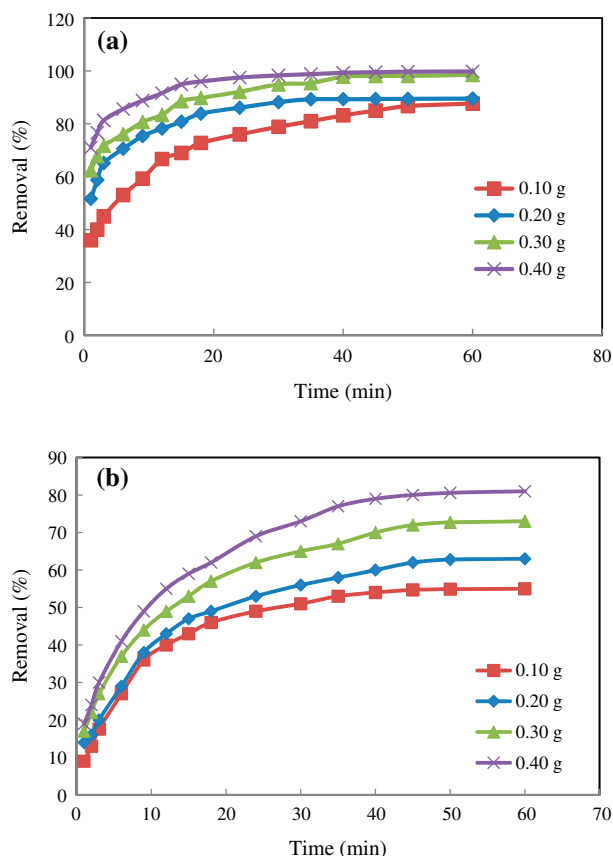


Fig. 9. Effect of contact time on the removal of (a) MB dye and (b) Pb²⁺ ion.

cess. In our case, four different kinetic models were applied in order to establish which of them shows the best fit with experimentally obtained data (Tables 5–8 for MB and Tables 9–12 for Pb²⁺ ions). The pseudo-first-order kinetic model is frequently used in kinetic studies [45]. It is expressed by the following equation:

$$\log(q_e - q_t) = \log(q_e) - (K_1/2.303)t \quad (9)$$

where K_1 (g mg⁻¹ min⁻¹) is the rate constant of pseudo-first-order adsorption, which is obtained from the slopes of the linear plots of $\log(q_e - q_t)$ vs. t (Tables 5–8 for MB and Tables 9–12 for Pb²⁺). The pseudo-second-order kinetic model may be expressed by the equation:

$$t/q_t = 1/K_2q_e^2 + (1/q_e)t \quad (10)$$

where K_2 (g mg⁻¹ min⁻¹) is the equilibrium rate constant for the pseudo-second-order adsorption and can be obtained from the plot of t/q_t against t (Tables 5–8

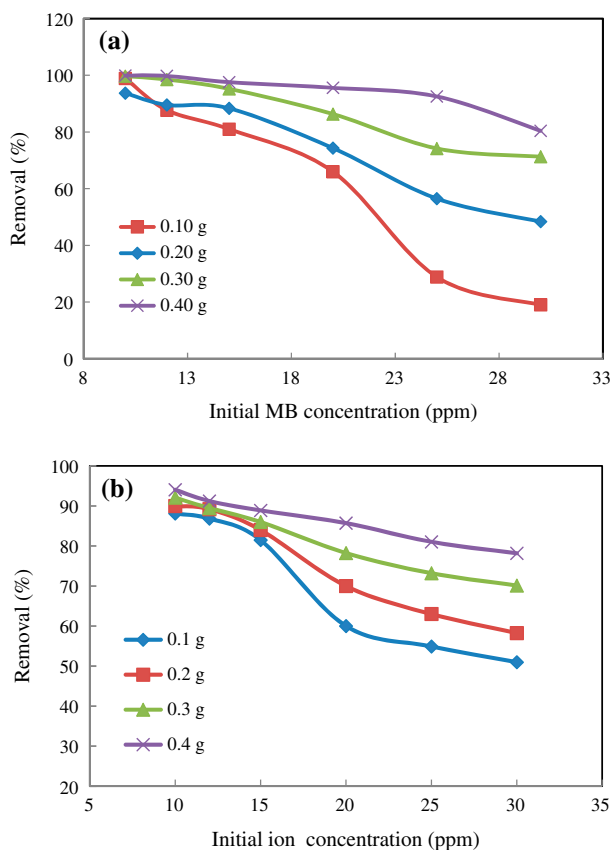


Fig. 10. Effect of initial dye concentration on the removal of (a) MB dye and (b) Pb^{2+} ion.

for MB and Tables 9–12 for Pb^{2+} ions) [46]. The Elovich model describes a number of reaction mechanisms, including bulk and surface diffusion and the activation and deactivation of catalytic surfaces (Tables 5–8 for MB and Tables 9–12 for Pb^{2+} ion) [47]. It is represented as:

$$q_t = 1/\beta \ln(\alpha\beta) + 1/\beta \ln(t) \quad (11)$$

where α ($\text{mg g}^{-1} \text{min}$) and β (g mg^{-1}) are the constants of adsorption and are determined as depicted. The intraparticle diffusion model is defined by the following equation:

$$q_t = K_{\text{id}} t^{1/2} + C \quad (12)$$

where K_{id} ($\text{g mg}^{-1} \text{min}^{-1}$) is the constant of adsorption and is determined from a plot of q_t vs. $t^{1/2}$. All the kinetic data for adsorption by AC-Tamarisk, calculated from the related plots, are summarized in Tables 5–8 for MB and Tables 9–12 for Pb^{2+} ions. The validity of

the exploited models is verified by R^2 . A comparison of the R^2 values for different models suggests that the pseudo-second-order kinetic model fits the best since it has the highest value ($R^2 = 1.0$ for Pb^{2+} ions and $R^2 = 0.9999$ for MB). The pseudo-second-order kinetic model implies that the predominant process is chemisorption, which involves sharing of electrons between the adsorbate and the surface of the adsorbent. Chemisorption is usually restricted to just one layer of molecules on the surface, although it may be followed by additional layers of physically adsorbed molecules [48].

3.9. Adsorption isotherms

Adsorption isotherm indicates how molecules of adsorbate are partitioned between the adsorbent and the liquid phase at equilibrium as a function of adsorbate concentration. In this study, equilibrium data obtained for the adsorption of Pb^{2+} ions and MB onto AC-Tamarisk were analyzed by considering the Langmuir, Freundlich, Dubinin–Radushkevich, and Temkin isotherm models. The theoretical Langmuir isotherm as one of the most traditional models has the maximum adsorption capacity corresponding to complete monolayer coverage on the adsorbent surface that is calculated according to the well-known procedure [49]. A plot of C_e/q_e vs. C_e at various amounts of AC in the range of 0.1–0.4 g should indicate a straight line with a slope of $1/Q_m$ and an intercept of $1/K_a Q_m$. Depicting this line under various conditions (amount of AC) makes it possible to calculate the value of the constant corresponding to this model (Table 13 for MB and Table 14 for Pb^{2+} ion). The high correlation coefficients and the high maximum monolayer capacity of 7.19 – 3.07 mg g^{-1} for MB and 7.74 – 3.52 for Pb^{2+} ions, respectively, are strong positive evidence on the fitness of equilibrium data of MB and Pb^{2+} ion adsorption according to the Langmuir model. The Freundlich isotherm model [49] has constants such as K_F that show information about the bonding energy and are known as the adsorption or distribution coefficient and represent the quantity of dye adsorbed onto the adsorbent, $1/n$ shows an adsorption intensity of dye onto the adsorbent (surface heterogeneity). The value closer to zero by rising the heterogeneous nature of surface ($1/n < 1$) indicates a normal Langmuir isotherm, while $1/n$ above one indicates a bi-mechanism and cooperative adsorption. The applicability of the Freundlich adsorption isotherm was assessed by plotting $\ln(q_e)$ vs. $\ln(C_e)$ and the respective values for these model constants at various amounts of the adsorbent are shown in Table 13 for MB and in Table 14 for Pb^{2+} ions. The correlation coefficients

Table 5

Kinetic parameters of MB adsorption onto AC: 0.1 g of adsorbent over 10–30 mg L⁻¹ under optimal conditions of other variables

Models	Parameters	Dye concentration (ppm)					
		10	12	15	20	25	30
First-order kinetic model $\log(q_e - q_t) = \log(q_e) - (K_1/2.303)t$	K_1	0.085	0.089	0.084	0.067	0.088	0.067
	$q_{e(\text{cal})}$	2.724	4.41	5.158	4.01	2.093	1.823
	R^2	0.9425	0.8664	0.8712	0.9234	0.9629	0.8328
Second-order kinetic model $t/q_t = 1/K_2q_e^2 + (1/q_e)t$	K_2	0.080	0.043	0.036	0.044	0.094	0.100
	$q_{e(\text{cal})}$	4.755	5.507	6.389	6.780	3.770	2.919
	R^2	0.999	0.9968	0.9955	0.9971	0.9980	0.9977
	h	1.808	1.408	1.456	2.044	1.340	0.854
Intraparticle diffusion $q_t = K_{\text{id}}t^{1/2} + C$	K_{dif}	0.356	0.471	0.561	0.524	0.279	0.885
	C	2.234	2.036	2.181	2.832	1.768	1.141
	R^2	0.8990	0.9463	0.9634	0.9229	0.9315	0.8854
Elovich $q_t = 1/\beta \ln(\alpha\beta) + 1/\beta \ln(t)$	β	1.554	1.204	1.021	1.029	2.033	2.224
	R^2	0.9879	0.9891	0.9853	0.9863	0.9755	0.9881
Experimental data	$q_{e(\text{exp})}$	4.6	5.265	6.08	6.25	3.615	2.865

Table 6

Kinetic parameters of MB adsorption onto AC: 0.2 g of adsorbent over 10–30 mg L⁻¹ under optimal conditions of other variables

Models	Parameters	Dye concentration (ppm)					
		10	12	15	20	25	30
First-order kinetic model $\log(q_e - q_t) = \log(q_e) - (K_1/2.303)t$	K_1	0.075	0.121	0.084	0.081	0.068	0.085
	$q_{e(\text{cal})}$	1.178	1.279	1.963	2.707	1.393	2.789
	R^2	0.9647	0.9850	0.7919	0.8637	0.9882	0.8417
Second-order kinetic model $t/q_t = 1/K_2q_e^2 + (1/q_e)t$	K_2	0.272	0.235	0.125	0.071	0.143	0.0072
	$q_{e(\text{cal})}$	2.38	2.76	3.37	3.85	3.61	3.77
	R^2	0.9995	0.9996	0.9982	0.9933	0.9985	0.9943
	h	1.54	1.798	1.427	1.054	1.858	1.026
Intraparticle diffusion $q_t = K_{\text{id}}t^{1/2} + C$	K_{dif}	0.1266	0.1586	0.2114	0.2693	0.1950	0.2725
	C	1.504	1.681	1.843	1.774	2.201	1.691
	R^2	0.8705	0.8595	0.9358	0.9925	0.9432	0.9864
Elovich $q_t = 1/\beta \ln(\alpha\beta) + 1/\beta \ln(t)$	β	4.307	3.42	2.66	2.204	2.897	2.17
	R^2	0.9851	0.9812	0.9947	0.9466	0.9940	0.9461
Experimental data	$q_{e(\text{exp})}$	2.35	2.69	3.32	3.72	3.55	3.63

($R^2 = 0.7615$ – 0.9541 for MB and $R^2 = 0.9956$ – 0.8444 for Pb^{2+} ions) and higher error values of this model show that the Freundlich model has lower efficiency compared to the Langmuir model. Although the Langmuir and even the Freundlich models have a reasonable

and acceptable value of R^2 , the applicability of other models such as Temkin isotherm has commonly been studied using the following linear form: The Temkin isotherm Eq. (13) can be simplified to the following equation:

Table 7

Kinetic parameters of MB adsorption onto AC: 0.3 g of adsorbent over 10–30 mg L⁻¹ under optimal conditions of other variables

Models	Parameters	Dye concentration (ppm)					
		10	12	15	20	25	30
First-order kinetic model $\log(q_e - q_t) = \log(q_e) - (K_1/2.303)t$	K_1	0.089	0.087	0.077	0.071	0.061	0.059
	$q_{e(cal)}$	1.28	1.52	2.09	2.15	1.21	2.28
	R^2	0.9777	0.9759	0.9353	0.9100	0.9427	0.9661
Second-order kinetic model $t/q_t = 1/K_2q_e^2 + (1/q_e)t$	K_2	0.514	0.287	0.156	0.094	0.077	0.066
	$q_{e(cal)}$	1.69	2.02	2.44	3.015	3.226	3.711
	R^2	0.9998	0.9991	0.9963	0.9904	0.9960	0.9923
	h	1.47	1.17	0.98	0.93	0.89	0.70
Intraparticle diffusion $q_t = K_{id}t^{1/2} + C$	K_{dif}	0.078	0.107	0.141	0.223	0.227	0.288
	C	1.15	1.26	1.37	1.76	2.02	2.49
	R^2	0.8487	0.9268	0.9849	0.9865	0.9743	0.9886
Elovich $q_t = 1/\beta \ln(\alpha\beta) + 1/\beta \ln(t)$	β	6.8	5.2	4.2	2.7	2.5	2.03
	R^2	0.9709	0.9892	0.9597	0.9137	0.9518	0.9647
Experimental data	$q_{e(exp)}$	1.66	1.995	2.385	2.88	3.095	3.6

Table 8

Kinetic parameters of MB adsorption onto AC: 0.4 g of adsorbent over 10–30 mg L⁻¹ under optimal conditions of other variables

Models	Parameters	Dye concentration (ppm)					
		10	12	15	20	25	30
First-order kinetic model $\log(q_e - q_t) = \log(q_e) - (K_1/2.303)t$	K_1	0.091	0.102	0.076	0.077	0.096	0.080
	$q_{e(cal)}$	7.186	2.395	1.336	1.830	1.792	1.241
	R^2	0.9086	0.9533	0.8821	0.8720	0.9255	0.9756
Second-order kinetic model $t/q_t = 1/K_2q_e^2 + (1/q_e)t$	K_2	1.887	0.726	0.319	0.192	0.139	0.172
	$q_{e(cal)}$	1.26	1.52	1.85	2.42	2.99	3.12
	R^2	1	0.9999	0.999	0.9987	0.9988	0.9994
	h	3.00	1.68	0.095	1.40	1.24	1.66
Intraparticle diffusion $q_t = K_{id}t^{1/2} + C$	K_{dif}	0.035	0.0592	0.0918	0.148	0.202	0.195
	C	1.0365	1.121	1.195	1.377	1.550	1.752
	R^2	0.7114	0.8423	0.9385	0.9246	0.9253	0.8752
Elovich $q_t = 1/\beta \ln(\alpha\beta) + 1/\beta \ln(t)$	β	14.75	9.12	6.15	3.79	2.78	2.79
	R^2	0.9048	0.9751	0.9903	0.9937	0.9910	0.9883
Experimental data	$q_{e(exp)}$	1.25	1.5	1.83	2.4	2.89	3.03

$$q_e = \beta \ln \alpha + \beta \ln C_e \tag{13}$$

where $\beta = (RT)/b$ is related to the heat of adsorption, T is the absolute temperature in Kelvin, and R is the universal gas constant, 8.314 (J mol⁻¹ K⁻¹). Adsorption

data were analyzed according to the linear form of the Temkin isotherm Eq. (13). An examination of the data shows that the Temkin isotherm is efficiently applicable for fitting MB and Pb²⁺ ion adsorption onto AC. The linear isotherm constants and coefficients of

Table 9

Kinetic parameters of Pb^{2+} ion adsorption onto AC: 0.1 g of adsorbent over 10–30 mg L⁻¹ under optimal conditions of other variables

Models	Parameters	Dye concentration (ppm)					
		10	12	15	20	25	30
First-order kinetic model $\log(q_e - q_t) = \log(q_e) - (K_1/2.303)t$	K_1	0.034	0.033	0.027	0.014	0.012	0.011
	$q_{e(cal)}$	3.52	4.36	5.44	7.56	9.52	12.21
	R^2	0.9707	0.9731	0.9428	0.8541	0.7997	0.8512
Second-order kinetic model $t/q_t = 1/K_2q_e^2 + (1/q_e)t$	K_2	0.028	0.021	0.017	0.020	0.018	0.012
	$q_{e(cal)}$	4.88	5.83	6.92	6.76	7.83	8.99
	R^2	0.9917	0.9917	0.9953	0.9980	0.9987	0.9982
	h	0.6691	0.7220	0.8314	0.9304	0.131	0.9665
Intraparticle diffusion $q_t = K_{id}t^{1/2} + C$	K_{dif}	0.5249	0.6422	0.7814	0.7593	0.8917	1.045
	C	0.8064	0.7871	0.8114	0.9784	0.1.1604	0.7648
	R^2	0.9661	0.9708	0.9560	0.9222	0.8927	0.9337
Elovich $q_t = 1/\beta \ln(\alpha\beta) + 1/\beta \ln(t)$	β	1.10	0.90	0.74	0.74	0.62	0.54
	R^2	0.9870	0.9838	0.9841	0.9871	0.9829	0.9860
Experimental data	$q_{e(exp)}$	4.99	5.99	7.49	9.97	12.45	14.94

Table 10

Kinetic parameters of Pb^{2+} ion adsorption onto AC: 0.2 g of adsorbent over 10–30 mg L⁻¹ under optimal conditions of other variables

Models	Parameters	Dye concentration (ppm)					
		10	12	15	20	25	30
First-order kinetic model $\log(q_e - q_t) = \log(q_e) - (K_1/2.303)t$	K_1	0.036	0.034	0.027	0.018	0.015	0.013
	$q_{e(cal)}$	1.681	2.063	2.485	3.735	4.670	5.787
	R^2	0.9789	0.9763	0.9454	0.9282	0.8780	0.8661
Second-order kinetic model $t/q_t = 1/K_2q_e^2 + (1/q_e)t$	K_2	0.064	0.050	0.047	0.032	0.031	0.026
	$q_{e(cal)}$	2.44	2.92	3.41	3.89	4.43	4.97
	R^2	0.9926	0.9931	0.9959	0.9919	0.9964	0.9959
	h	0.3807	0.4272	0.5487	0.4876	0.6072	0.6487
Intraparticle diffusion $q_t = K_{id}t^{1/2} + C$	K_{dif}	0.2572	0.3095	0.3600	0.4300	0.4934	0.5622
	C	0.5026	0.5348	0.6892	0.5324	0.6560	0.6502
	R^2	0.9645	0.9615	0.9460	0.9586	0.9367	0.9403
Elovich $q_t = 1/\beta \ln(\alpha\beta) + 1/\beta \ln(t)$	β	2.28	1.86	1.58	1.34	1.55	1.02
	R^2	0.9894	0.9920	0.9954	0.9811	0.9821	0.9779
Experimental data	$q_{e(exp)}$	2.49	2.99	3.74	4.99	6.23	7.47

determination are presented in Table 13 for MB and in Table 14 for Pb^{2+} ions. The heat of MB and Pb^{2+} ion adsorption onto AC was found to increase from 0.2804 to 0.8664 kJ mol⁻¹ for MB and from 0.734 to 0.994 kJ mol⁻¹ for Pb^{2+} ions with a decrease in AC

dose from 0.1 to 0.4 g. The R^2 obtained from the Temkin model was comparable to that obtained from Langmuir and Freundlich equations, which explain the applicability of Temkin model to the adsorption of MB and Pb^{2+} ions onto AC-Tamarisk. The D–R model

Table 11

Kinetic parameters of Pb²⁺ ion adsorption onto AC: 0.3 g of adsorbent over 10–30 mg L⁻¹ under optimal conditions of other variables

Models	Parameters	Dye concentration (ppm)					
		10	12	15	20	25	30
First-order kinetic model $\log(q_e - q_t) = \log(q_e) - (K_1/2.303)t$	K_1	0.089	0.087	0.077	0.071	0.061	0.059
	$q_{e(\text{cal})}$	1.28	1.52	2.09	2.15	1.21	2.28
	R^2	0.9777	0.9759	0.9353	0.9100	0.9427	0.9661
Second-order kinetic model $t/q_t = 1/K_2q_e^2 + (1/q_e)t$	K_2	0.514	0.287	0.156	0.094	0.077	0.066
	$q_{e(\text{cal})}$	1.69	2.02	2.44	3.015	3.226	3.711
	R^2	0.9998	0.9991	0.9963	0.9904	0.9960	0.9923
	h	1.47	1.17	0.98	0.93	0.89	0.70
Intraparticle diffusion $q_t = K_{\text{id}}t^{1/2} + C$	K_{dif}	0.078	0.107	0.141	0.223	0.227	0.288
	C	1.15	1.26	1.37	1.76	2.02	2.49
	R^2	0.8487	0.9268	0.9849	0.9865	0.9743	0.9886
Elovich $q_t = 1/\beta \ln(\alpha\beta) + 1/\beta \ln(t)$	β	6.8	5.2	4.2	2.7	2.5	2.03
	R^2	0.9709	0.9892	0.9597	0.9137	0.9518	0.9647
Experimental data	$q_{e(\text{exp})}$	1.66	1.995	2.385	2.88	3.095	3.6

Table 12

Kinetic parameters of Pb²⁺ ion adsorption onto AC: 0.4 g of adsorbent over 10–30 mg L⁻¹ under optimal conditions of other variables

Models	Parameters	Dye concentration (ppm)					
		10	12	15	20	25	30
First-order kinetic model $\log(q_e - q_t) = \log(q_e) - (K_1/2.303)t$	K_1	0.044	0.038	0.034	0.032	0.027	0.025
	$q_{e(\text{cal})}$	1.41	1.15	1.13	1.66	2.12	2.66
	R^2	0.9612	0.9531	0.9435	0.9495	0.9247	0.9258
Second-order kinetic model $t/q_t = 1/K_2q_e^2 + (1/q_e)t$	K_2	0.183	0.147	0.110	0.066	0.053	0.041
	$q_{e(\text{cal})}$	1.26	1.47	1.80	2.38	2.83	3.30
	R^2	0.9973	0.9970	0.9971	0.9943	0.9958	0.9947
	h	0.2893	0.3188	0.3566	0.3733	0.4275	0.4435
Intraparticle diffusion $q_t = K_{\text{id}}t^{1/2} + C$	K_{dif}	0.1189	0.1418	0.01806	0.2515	0.3068	0.3657
	C	0.3888	0.4275	0.4667	0.4670	0.5002	0.4833
	R^2	0.9346	0.9333	0.9332	0.9569	0.9471	0.9541
Elovich $q_t = 1/\beta \ln(\alpha\beta) + 1/\beta \ln(t)$	β	4.76	3.98	3.13	2.28	1.86	1.57
	R^2	0.9825	0.9866	0.9861	0.9828	0.9876	0.9830
Experimental data	$q_{e(\text{exp})}$	1.25	1.49	1.87	2.49	3.12	3.74

was also applied to estimate the porosity, free energy, and characteristics of adsorbents [50]. The D–R isotherm does not assume a homogeneous surface or

constant adsorption potential. The D–R model has commonly been applied in Eq. (14) and its linear form can be shown in Eq. (15):

Table 13

Isotherm constant parameters and coefficient of determination calculated for the adsorption of MB onto AC-Tamarisk

Isotherm	Equation	Parameters	Amount of adsorbent (g)			
			0.1	0.2	0.3	0.4
Langmuir	$C_e/q_e = 1/K_a Q_m + C_e/Q_m$	Q_m (mg g ⁻¹)	7.19	3.69	3.55	3.07
		K_a (L mg ⁻¹)	2.35	3.47	3.91	8.04
		R_L	0.04–0.01	0.03–0.01	0.025–0.01	0.01–0.004
		R^2	0.9952	0.9990	0.9957	0.9980
Freundlich	$\ln q_e = \ln K_F + (1/n) \ln C_e$	$1/n$	0.147	0.128	0.136	0.139
		K_F (L mg ⁻¹)	4.96	2.71	2.58	2.41
		R^2	0.8933	0.7615	0.9871	0.9541
Temkin	$q_e = B_1 \ln K_T + B_1 \ln C_e$	B_1	0.8664	0.3879	0.3345	0.2804
		K_T (L mg ⁻¹)	306.14	1,187.87	2,944.64	6,956.01
		R^2	0.8884	0.7721	0.9637	0.9242
Dubinin and Radushkevich	$\ln q_e = \ln Q_s - K\varepsilon^2$	Q_s (mg g ⁻¹)	6.81	3.59	2.92	2.54
		K	-1E-07	-8E-08	-8E-09	-5E-09
		E (kJ mol ⁻¹) $= 1/(2K)^{1/2}$	2.2	2.5	7.9	10.0
		R^2	0.8719	0.8992	0.7127	0.8066

Table 14

Isotherm constant parameters and coefficient of determination calculated for the adsorption of Pb²⁺ ions onto AC-Tamarisk

Isotherm	Equation	Parameters	Amount of adsorbent (g)			
			0.1	0.2	0.3	0.4
Langmuir	$C_e/q_e = 1/K_a Q_m + C_e/Q_m$	Q_m (mg g ⁻¹)	7.74	4.60	3.95	3.52
		K_a (L mg ⁻¹)	0.945	0.836	0.617	0.606
		R_L	0.03–0.09	0.04–0.11	0.05–0.12	0.05–0.14
		R^2	0.9832	0.9912	0.9832	0.9840
Freundlich	$\ln q_e = \ln K_F + (1/n) \ln C_e$	$1/n$	0.1689	0.2286	0.3291	0.3898
		K_F (L mg ⁻¹)	4.64	2.41	1.66	1.39
		R^2	0.8444	0.9562	0.9956	0.9943
Temkin	$q_e = B_1 \ln K_T + B_1 \ln C_e$	B_1	0.994	0.777	0.740	0.734
		K_T (L mg ⁻¹)	119.4	25.37	8.06	6.72
		R^2	0.8462	0.9660	0.9753	0.9730
Dubinin and Radushkevich	$\ln q_e = \ln Q_s - K\varepsilon^2$	Q_s (mg g ⁻¹)	6.88	3.92	2.94	2.42
		K	-2E-07	-2E-07	-2E-07	-1E-07
		E (kJ mol ⁻¹) $= 1/(2K)^{1/2}$	1.58	1.58	1.58	2.24
		R^2	0.8601	0.9122	0.8263	0.7914

$$q_e = Q_m \exp(-B\varepsilon^2) \quad (14)$$

$$\ln q_e = \ln Q_m - B\varepsilon^2 \quad (15)$$

where B is a constant related to the adsorption energy, Q_m is the theoretical saturation capacity, and ε is the Polanyi potential calculated from Eq. (16):

$$\varepsilon = RT \ln(1 + 1/C_e) \quad (16)$$

The slope of the plot of $\ln q_e$ vs. ε^2 gives B (mol² (kJ²)⁻¹) and the intercept yields the adsorption capacity, Q_m (mg g⁻¹). The mean free energy of adsorption (E) for the transfer of one mole of target

from infinity in solution to the surface of the solid was calculated from the B value using the following relation [51]:

$$E = 1/\sqrt{2B} \quad (17)$$

The calculated value of D-R (Table 13 for MB and Table 14 for Pb^{2+}) shows that the model saturation adsorption capacity under optimum conditions using different amounts of adsorbents was in the range of 6.81–2.54 for MB and 6.88–2.42 for Pb^{2+} ions, respectively, which is in good agreement with the respective Langmuir value. The values of E calculated using Eq. (17) are 2.2–10.0 kJ mol^{-1} for MB and 1.58–2.24 kJ mol^{-1} for Pb^{2+} corresponding to the physico-sorption process which plays a significant role in the adsorption of MB and Pb^{2+} ions onto AC. The lower R^2 of the Freundlich model in comparison to the Langmuir model suggests that the removal process is better modeled by monolayer compared to multilayer adsorption. To confirm this result, the favorable or unfavorable MB and Pb^{2+} ion adsorption using the Langmuir model was judged by the calculation of the separation factor (R_L) as follows [52]:

$$R_L = 1/(1 + K_a C_0) \quad (18)$$

where K_a (L mg^{-1}) is the Langmuir constant and C_0 (mg L^{-1}) is the initial concentration. The adsorption process can be determined as favorable when the R_L value lies between zero and one. It was found that for all adsorbent dosages and initial MB and Pb^{2+} ion concentrations, the R_L value is lower than one, which suggests the favorable adsorption and good fitness of the Langmuir model to explain experimental data. On the other hand, an increase in the R_L value with rising initial MB and Pb^{2+} ion concentrations and adsorbent dosage shows the high tendency of MB and Pb^{2+} ions for adsorption onto AC.

4. Conclusion

AC from the wood of Tamarisk has been prepared and used as an effective adsorbent for the removal of MB and Pb^{2+} ions from aqueous solutions. In the present investigation, the RF model has been developed as an efficient tool for the prediction of MB and Pb^{2+} ion adsorption onto AC obtained from Tamarisk. The results show that there is a good agreement between the experimental data and predicted data using the presented RF model. The effects of adsorbent dosage, initial pH, contact time, and initial dye and ion concentrations on the removal of dye and ion were

investigated through batch experiments. Optimum dosage, pH, and contact time for AC were obtained to be 0.3 g, pH 5, and 30 min, respectively, and for MB were obtained to be 0.3 g, pH 5, and 60 min, respectively. Isotherm modeling revealed that the Langmuir equation could better describe the adsorption of dye and ion onto AC as compared to other models. The adsorption kinetics can be successfully fitted to the pseudo-second-order kinetic model. The results of the intraparticle diffusion model suggested that intraparticle diffusion was not the only rate-controlling step. In view of these results, it can be concluded that AC can be utilized as a low-cost and effective adsorbent in the removal of MB and Pb^{2+} ions from aqueous solutions.

References

- [1] B. Volesky (Ed.), Removal and Recovery of Heavy Metals by Biosorption of Heavy Metals, CRC Press, Boca Raton, FL, 1990, pp. 3–43.
- [2] W. Lo, H. Chua, K.H. Lam, S.H. Bi, A comparative investigation on the biosorption of lead by filamentous fungal biomass, Chemosphere 39 (1999) 2723–2736.
- [3] K. Li, X. Wang, Adsorptive removal of Pb(II) by activated carbon prepared from *Spartina alterniflora*: Equilibrium, kinetics and thermodynamics, Bioresour. Technol. 100 (2009) 2810–2815.
- [4] Ö. Gerçel, H.F. Gerçel, Adsorption of lead(II) ions from aqueous solutions by activated carbon prepared from biomass plant material of *Euphorbia rigida*, Chem. Eng. J. 132 (2007) 289–297.
- [5] T.V.N. Padmesh, K. Vijayaraghavan, G. Sekaran, M. Velan, Biosorption of Acid Blue 15 using fresh water macroalga *Azolla filiculoides*: Batch and column studies, Dyes Pigm. 71 (2006) 77–82.
- [6] Y.S. Ho, T.H. Chiang, Y.M. Hsueh, Removal of basic dye from aqueous solution using tree fern as a biosorbent, Process Biochem. 40 (2005) 119–124.
- [7] A.H. Sulaymon, B.A. Abid, J.A. Al-Najar, Removal of lead copper chromium and cobalt ions onto granular activated carbon in batch and fixed-bed adsorbers, Chem. Eng. J. 155 (2009) 647–653.
- [8] K.G. Sreejalekshmi, K. Krishnan, T.S. Anirudhan, Adsorption of Pb(II) and Pb(II)-citric acid on sawdust activated carbon: Kinetic and equilibrium isotherm studies, J. Hazard. Mater. 161 (2009) 1506–1513.
- [9] M. Goyal, S. Singh, R.C. Bansal, Equilibrium and dynamic adsorption of methylene blue from aqueous solutions by surface modified activated carbons, Carbon Sci. 5 (2004) 170–179.
- [10] F.K. Bangash, A. Manaf, Dyes removal from aqueous solution using wood activated charcoal of Bombax cieba tree, J. Chin. Chem. Soc. 52 (2005) 489–494.
- [11] E. Lorencgrabowska, G. Gryglewicz, Adsorption characteristics of Congo Red on coal-based mesoporous activated carbon, Dyes Pigm. 74 (2007) 34–40.
- [12] C. Namasivayam, D. Kavitha, Removal of Congo Red from water by adsorption onto activated carbon prepared from coir pith, an agricultural solid waste, Dyes Pigm. 54 (2002) 47–58.

- [13] R.L. Teng, F.C. Wu, R.S. Juang, Liquid-phase adsorption of dyes and phenols using pinewood-based activated carbons, *Carbon* 41 (2003) 487–495.
- [14] B.K. Singh, N.S. Rawat, Comparative sorption equilibrium studies of toxic phenols on flyash and impregnated flyash, *J. Chem. Technol. Biotechnol.* 61 (1994) 307–317.
- [15] A. Aygün, S. Yenisoy-Karakaş, I. Duman, Production of granular activated carbon from fruit stones and nutshells and evaluation of their physical, chemical and adsorption properties, *Microporous Mesoporous Mater.* 66 (2003) 189–195.
- [16] C. Yang Yin, M. Kheireddine Aroua, W. Mohd Ashri Wan Daud, Review of modifications of activated carbon for enhancing contaminant uptakes from aqueous solutions, *Sep. Purif. Technol.* 52 (2007) 403–415.
- [17] M. Ghaedi, A. Ansari, M.H. Habibi, A.R. Asghari, Removal of malachite green from aqueous solution by zinc oxide nanoparticle loaded on activated carbon: Kinetics and isotherm study, *J. Ind. Eng. Chem.* 20 (2014) 17–28.
- [18] I. Salame, T. Bandosz, Surface chemistry of activated carbons: Combining the results of temperature-programmed desorption, Boehm, and potentiometric titrations, *J. Colloid Interface Sci.* 240 (2001) 252–258.
- [19] D.J. Malik, V. Strelko Jr., M. Streat, A.M. Puziy, Characterisation of novel modified active carbons and marine algal biomass for the selective adsorption of lead, *Water Res.* 36 (2002) 1527–1538.
- [20] V. Boonamnuayvitaya, C. Chaiya, W. Tanthapanichakoon, S. Jarudilokkul, Removal of heavy metals by adsorbent prepared from pyrolyzed coffee residues and clay, *Sep. Purif. Technol.* 35 (2004) 11–22.
- [21] L.A. Teles de Vasconcelos, C.G. Gonzalez Beca, Adsorption equilibria between pine bark and several ions in aqueous solution, 1. Pb(II), *Eur. Water Pollut. Control* 4 (1994) 41–51.
- [22] M. Ahmedna, W.E. Marshall, A.A. Hussein, R.M. Rao, I. Goktepe, The use of nutshell carbons in drinking water filters for removal of trace metals, *Water Res.* 38 (2004) 1062–1068.
- [23] A.H. El-Sheikh, A.P. Newman, H.K. Al-Daffae, S. Phull, N. Cresswell, Characterization of activated carbon prepared from a single cultivar of Jordanian Olive stones by chemical and physicochemical techniques, *J. Anal. Appl. Pyrol.* 71 (2004) 151–164.
- [24] M. Ghaedi, A.M. Ghaedi, M. Hossainpour, A. Ansari, M.H. Habibi, A.R. Asghari, Least square-support vector (LS-SVM) method for modeling of methylene blue dye adsorption using copper oxide loaded on activated carbon: Kinetic and isotherm study, *J. Ind. Eng. Chem.* 20 (2014) 1641–1649.
- [25] M. Ghaedi, R. Hosaininia, A. Ghaedi, A. Vafaei, F. Taghizadeh, Adaptive neuro-fuzzy inference system model for adsorption of 1,3,4-thiadiazole-2,5-dithiol onto gold nanoparticles-activated carbon, *Spectrochim. Acta A Mol. Biomol. Spectrosc.* 131 (2014) 606–614.
- [26] M. Ghaedi, N. Zeinali, A.M. Ghaedi, M. Teimuori, J. Tashkhourian, Artificial neural network-genetic algorithm based optimization for the adsorption of methylene blue and brilliant green from aqueous solution by graphite oxide nanoparticle, *Spectrochim. Acta A Mol. Biomol. Spectrosc.* 125 (2014) 264–277.
- [27] M. Ghaedi, A. Ghaedi, A. Ansari, F. Mohammadi, A. Vafaei, Artificial neural network and particle swarm optimization for removal of methyl orange by gold nanoparticles loaded on activated carbon and Tamarisk, *Spectrochim. Acta A Mol. Biomol. Spectrosc.* 132 (2014) 639–654.
- [28] M. Ghaedi, A.M. Ghaedi, E. Negintaji, A. Ansari, A. Vafaei, M. Rajabi, Random forest model for removal of bromophenol blue using activated carbon obtained from *Astragalus bisulcatus* tree, *J. Ind. Eng. Chem.* 20 (2014) 1793–1803.
- [29] A. Philibert, C. Loyce, D. Makowski, Prediction of N₂O emission from local information with Random Forest, *Environ. Pollut.* 177 (2013) 156–163.
- [30] M.H. Schwartz, A. Rozumalski, W. Truong, T.F. Novacheck, Predicting the outcome of intramuscular psoas lengthening in children with cerebral palsy using preoperative gait data and the random forest algorithm, *Gait. Posture.* 37 (2013) 473–479.
- [31] S. Adusumilli, D. Bhatt, H. Wang, P. Bhattacharya, V. Devabhaktuni, A low-cost INS/GPS integration methodology based on random forest regression, *Expert Syst. Appl.* 40 (2013) 4653–4659.
- [32] L. Breiman, Random forests, *MLear* 45 (2001) 5–32.
- [33] B. Samiey, A.R. Toosi, Adsorption of malachite green on silica gel: Effects of NaCl, pH and 2-propanol, *J. Hazard. Mater.* 184 (2010) 739–745.
- [34] M. Ghaedi, A. Ansari, F. Bahari, A.M. Ghaedi, A. Vafaei, A hybrid artificial neural network and particle swarm optimization for prediction of removal of hazardous dye brilliant green from aqueous solution using zinc sulfide nanoparticle loaded on activated carbon, *Spectrochim. Acta Part A Mol. Biomol. Spectrosc.* 137 (2015) 1004–1015.
- [35] M. Kobya, E. Demirbas, E. Senturk, M. Ince, Adsorption of heavy metal ions from aqueous solutions by activated carbon prepared from apricot stone, *Bioresour. Technol.* 96 (2005) 1518–1521.
- [36] B.H. Hameed, M.I. El-Khaiary, Batch removal of malachite green from aqueous solutions by adsorption on oil palm trunk fibre: Equilibrium isotherms and kinetic studies, *J. Hazard. Mater.* 154 (2008) 237–244.
- [37] C.P. Pradeep Sekhar, S. Kalidhasan, V. Rajesh, N. Rajesh, Bio-polymer adsorbent for the removal of malachite green from aqueous solution, *Chemosphere* 77 (2009) 842–847.
- [38] M. Ghaedi, A. Ansari, R. Sahraei, ZnS: Cu nanoparticles loaded on activated carbon as novel adsorbent for kinetic, thermodynamic and isotherm studies of Reactive Orange 12 and Direct yellow 12 adsorption, *Spectrochim. Acta Part A Mol. Biomol. Spectrosc.* 114 (2013) 687–694.
- [39] K. Ahmadi, M. Ghaedi, A. Ansari, Comparison of nickel doped zinc sulfide and/or palladium nanoparticle loaded on activated carbon as efficient adsorbents for kinetic and equilibrium study of removal of Congo Red dye, *Spectrochim. Acta Part A Mol. Biomol. Spectrosc.* 136 (2015) 1441–1449.
- [40] K. Kadirvelu, M. Palanival, R. Kalpana, S. Rajeswari, Activated carbon from an agricultural by-product, for the treatment of dyeing industry wastewater, *Bioresour. Technol.* 74 (2000) 263–265.
- [41] V.K. Garg, R. Gupta, A. Bala Yadav, R. Kumar, Dye removal from aqueous solution by adsorption on treated sawdust, *Bioresour. Technol.* 89 (2003) 121–124.

- [42] N. Kannan, M. Meenakshisundaram, Adsorption of Congo Red on various activated carbons, *Water Air Soil Pollut.* 138 (2002) 289–305.
- [43] M. Horsfall Jnr, A.I. Spiff, Effects of temperature on the sorption of Pb^{2+} and Cd^{2+} from aqueous solution by *Caladium bicolor* (Wild Cocoyam) biomass, *Electron. J. Biotechnol.* 8 (2005) 43–50.
- [44] K. Selvi, S. Pattabhi, K. Kadirvelu, Removal of Cr(VI) from aqueous solution by adsorption onto activated carbon, *Bioresour. Technol.* 80 (2001) 87–89.
- [45] B.H. Hameed, A.L. Ahmad, K.N.A. Latiff, Adsorption of basic dye (methylene blue) onto activated carbon prepared from rattan sawdust, *Dyes Pigm.* 75 (2007) 143–149.
- [46] A.S. Franca, L.S. Oliveira, M.E. Ferreira, Kinetics and equilibrium studies of methylene blue adsorption by spent coffee grounds, *Desalination* 249 (2009) 267–272.
- [47] F. Wu, R. Tseng, R. Juang, Characteristics of Elovich equation used for the analysis of adsorption kinetics in dye–chitosan systems, *Chem. Eng. J.* 150 (2009) 366–373.
- [48] E.N. El Qada, S.J. Allen, G.M. Walker, Adsorption of Methylene Blue onto activated carbon produced from steam activated bituminous coal: A study of equilibrium adsorption isotherm, *Chem. Eng. J.* 124 (2006) 103–110.
- [49] H.B. Senturk, D. Ozdes, A. Gundogdu, C. Duran, M. Soylak, Removal of phenol from aqueous solutions by adsorption onto organomodified Tirebolu bentonite: Equilibrium, kinetic and thermodynamic study, *J. Hazard. Mater.* 172 (2009) 353–362.
- [50] S. Lagergren, Zur theorie der sogenannten adsorption gelöster stoffe (About the theory of so-called adsorption of soluble substances), *Kung Sven. Vetén. Hand.* 24 (1898) 1–39.
- [51] D. Kavitha, C. Namasivayam, Experimental and kinetic studies on methylene blue adsorption by coir pith carbon, *Bioresour. Technol.* 98 (2007) 14–21.
- [52] M. Ghaedi, A.M. Ghaedi, E. Negintaji, A. Ansari, F. Mohammadi, Artificial neural network–imperialist competitive algorithm based optimization for removal of sunset yellow using $Zn(OH)_2$ nanoparticles-activated carbon, *J. Ind. Eng. Chem.* 20 (2014) 4332–4343.